The Astrophysical Journal, 712:445–452, 2010 March 20 doi:10.1088/0004-637X/712/1/445

ELECTRON-DRIVEN REACTIONS IN PROTO-PLANETARY ATMOSPHERES: METASTABLE ANIONS OF GASEOUS o-BENZYNE

F. Carelli[1], F. Sebastianelli[1], I. Baccarelli[1,2], and F. A. Gianturco[1,3]
[1] Department of Chemistry and INFM, University of Rome "La Sapienza," P.le Aldo Moro 5, 00185 Rome, Italy
[2] CASPUR Supercomputing Consortium, via dei Tizii 6, 00185 Rome, Italy
Received 2009 November 18; accepted 2010 January 27; published 2010 March 3

ABSTRACT

In this paper, we present an investigation into low-energy electron scattering ($E < 15$ eV) processes from a specific benzene-like polyatomic target such as ortho-benzyne, o-$C_6H_4(^1\Sigma)$, in order to gain a better understanding of the effects that possible low-lying metastable electron-attachment states could have on its nuclear fragmentation dynamics. The current importance of the dynamical evolution of this molecule lies in the fact that o-C_6H_4 is considered to be relevant for the circumstellar synthesis of large polycyclic aromatic hydrocarbons (PAHs), as a precursor for C_6H_6 production via ion-based ring closure reaction from C_2H_2. Our parameter-free scattering calculations are performed within the molecular reference frame, where we obtain the metastable anionic states for the nuclear equilibrium configuration and further characterize the properties of such transient anions with respect to those found earlier for the benzene molecule. Our quantum studies indicate that o-C_6H_4 is a more efficient producer of compact, fairly long-lived anionic intermediates than benzene itself; hence, this should more rapidly enter the chemical reaction cycles of PAHs formation, thereby disappearing from possible direct observation as a stable anion.

Key words: astrochemistry – circumstellar matter – molecular processes

Online-only material: color figures

1. INTRODUCTION

In a carbon-rich red giant or in a proto-planetary nebula (PPN) atmosphere, the major carbon-bearing chemical species that is initially formed is acetylene (C_2H_2), rather than the carbon monomer, due in principle to the wide availability of hydrogen. Specific chemical reactions, depending on both density and temperature conditions, could then lead to the formation of planar molecules of polycyclic aromatic hydrocarbons (PAHs), large aromatic molecules with five- or six-membered carbonaceous rings. Due to their marked electronic delocalization, they are very stable against photodissociation, and thus they could also be present in circumstellar environments. In fact, they are good candidates for the small grains produced in asymptotic giant branch (AGB) C-rich outflows and thus they have been proposed as potential carriers (they were and are the best candidates) for both the unidentified infrared bands and the diffuse interstellar bands, since these compounds in general show characteristic frequencies of absorption (Tielens 2005). Unfortunately, although significant laboratory spectroscopic work has been done and dedicated to PAHs in order to support the astronomical observations, their identification has always been elusive. Only benzene has been detected (Cernicharo et al. 2001) toward the PPN CRL 618, since the ν_4 bending mode (the strongest infrared feature for C_6H_6) was observed, and consequently the column density as well as the kinetic temperature was determined to be respectively of 5×10^{15} cm^{-2} and of 200 K. The discovery of benzene molecules (Cernicharo et al. 2001), which had never been found outside the solar system, thus represents a fundamental step toward our understanding of the possible interstellar and/or circumstellar synthesis of PAHs because of its being the simplest, basic aromatic unit. Moreover, the detection of circumstellar benzene molecules indicates that both physical and chemical conditions in PPN CRL 618 are right to activate a rich and diverse chemistry. This PPN in fact is an evolved object with a central B0 star (Sanchez Contreras & Sahai 2002; $T_* = 30{,}000$ K) and an ultracompact H II region surrounded by a carbon-rich (C/O > 1) molecular envelope (Sanchez Contreras & Sahai 2002). In addition, it shows optical high-velocity bipolar outflows as well as a low-velocity expanding torus (Sanchez Contreras & Sahai 2004), the latter being characterized by an intense molecular emission by means of which it has been possible to realize a rich molecular inventory including a large variety of hydrocarbons (Sanchez Contreras & Sahai 2004; Pardo et al. 2007). It follows then that either the UV photons from the rapidly evolving B0 central object or the strong shocks associated with the high-velocity stellar winds (up to 200 km s^{-1}) could in principle drive the polymerization of acetylene and consequently form benzene as the starting point for PAHs' synthesis. In fact, the interstellar/circumstellar chemical formation of large aromatic species has been modeled for the outflows of AGB stars in strong analogy with soot formation processes which take place in terrestrial combustion environments (Cherchneff et al. 1992; Frenklack & Feigelson 1989) as well as in a complex chain of reactions driven by photoionization and dissociative electron recombination (Woods et al. 2002).

The carbon-rich nature of PPN CRL 618, coupled with the C_6H_6, C_6H_2, and C_4H_2 detections (Cernicharo et al. 2001), makes it an excellent target for additional benzene derivative searches, although no spectral features associated with o-C_6H_4 have yet been detected toward this object (Widicus Weaver et al. 2007). Keeping in mind that we therefore do not have as yet reliable predictions of C_6H_6, C_6H_5, and o-C_6H_4 abundances in PPN (i.e., on the key species involved in the ionic and in radical-molecule reaction mechanisms as those shown in Figure 1), new observations and better theoretical data on both C_6H_5 and o-C_6H_4 would yield, in principle, important indicators as well as new insight into future modeling efforts. We present

[3] Author to whom any correspondence should be addressed: fa.gianturco@caspur.it

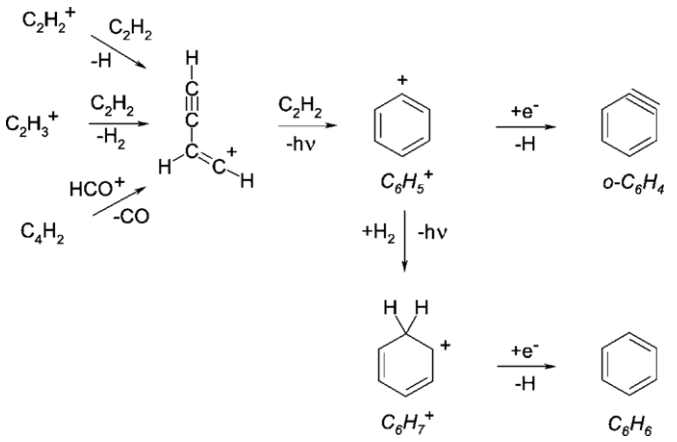

Figure 1. Ion-based reaction scheme for PPN benzene chemistry (adapted from Woods et al. 2002) in which the o-C_6H_4 is suggested as an actual competitor to benzene, thus leading to the larger PAHs.

here a study directed at providing one of the possible reasons for which the ortho-benzyne molecule might not have been detected during searches over CRL 618 (Widicus Weaver et al. 2007), despite of its large electric dipole moment of 1.68 D (Kraka & Cremer 1993) and of its lack of hyperfine splitting features, both of which would make it a very good candidate for detection with infrared and microwave spectroscopy. One could say, at least qualitatively, that a molecular system such as o-C_6H_4 is likely to be present in the torus of CRL 618, where higher densities could shield it from photodissociation as well as photoionization, while at the same time allowing its reaction with low-energy thermalized electrons, present in that environment (Sanchez Contreras & Sahai 2002), to form the corresponding metastable resonant anion. Our study is further encouraged by the fact that three molecular anions such as C_4H^-, C_6H^-, and C_8H^- have recently been detected (and in large quantities) in the envelope of the carbon-rich AGB star IRC+10216 (McCarthy et al. 2006; Sakai et al. 2007; Agundez et al. 2008), the latter being considered the AGB archetype. The possibility that a not so small but marginal fraction of interstellar molecular material might be in the form of anions was first suggested by Herbst (1981) in relation to carbon chains and other radicals with electron affinities large enough to exhibit in principle large radiative attachment rate. This characteristic is linked to the fact that the higher the electron affinity of a molecule, the more states are accessible for redistribution of the excess energy carried by the attached electron while, at the same time, autoionization is less likely to occur before the competing radiative stabilization of the excited anions could take place. Thus, the question we wish to address here is the possible existence of metastable anions of o-C_6H_4 as "doorway states" which can lead to ionic reaction chains on the way to the formation of increasingly more complex PAH species.

2. THE COMPUTATIONAL MODELING

2.1. Scattering Equations in a Single Center Expansion

The molecular quantum dynamical method we use in this study has been described in much more detail previously (Lucchese & Gianturco 1996), and only present an outline of it here. We perform the overall electron–molecule quantum scattering process in the time-independent framework within the Born–Oppenheimer approximation. The total wave function of the molecular target is expressed as an antisymmetrized product of electronic wave functions from Hartree–Fock orbitals of the neutral ground-state species, where the N molecular electrons are considered as keeping their ground-state configuration during the scattering process. It means that no core-excited resonances are initially involved, so that the scattering processes under investigation are limited to the elastic channels. Our computational approach is based on the single center expansion (SCE) of the electrons and nuclei so that the orbitals involved as well as the interaction potentials are expanded in a set of symmetry-adapted angular functions around the center of mass of the molecule; hence, any arbitrary three-dimensional function describing a given electron, either a bound or a scattering electron, originates at the molecular center of mass in which we also place the origin of the body-fixed frame of reference for the scattering process:

$$F^{p\mu}(r, \hat{\mathbf{r}}|\mathbf{R}) = \sum_{l,h} r^{-1} f_{lh}^{p\mu}(r|\mathbf{R}) X_{lh}^{p\mu}(\hat{\mathbf{r}}). \quad (1)$$

The indices refer to the μth component of the pth irreducible representation (IR) of the point group to which, at the nuclear geometry $\mathbf{R}$, the molecule belongs. The angular functions $X_{lh}^{p\mu}(\hat{\mathbf{r}})$ are symmetry-adapted angular functions given by the proper combination of spherical harmonics $Y_{lm}(\hat{\mathbf{r}})$:

$$X_{lh}^{p\mu}(\hat{\mathbf{r}}) = \sum_{m} b_{lmh}^{p\mu} Y_{lm}(\hat{\mathbf{r}}). \quad (2)$$

The coefficients $b_{lmh}^{p\mu}$ are discussed in the literature and can be obtained from a knowledge of the character tables of the relevant molecular point group (Altman & Herzig 1994). The coupled, partial integrodifferential scattering equations take the form

$$\left[\frac{d^2}{dr^2} - \frac{l(l+1)}{r^2} + 2(E - \epsilon_\alpha)\right] f_{lh}^{p\mu\alpha}(r|\mathbf{R}) = 2 \sum_{l'h'p'\mu'\alpha'} \int dr' V_{lh,l'h'}^{p\mu\alpha,p'\mu'\alpha'}(r, r'|\mathbf{R}) f_{l'h'}^{p'\mu'\alpha'}(r'|\mathbf{R}), \quad (3)$$

where E is the collision energy and ϵ_α is the electronic eigenvalue for the αth asymptotic state so that $k_\alpha^2/2 = E - \epsilon_\alpha$, where k_α is the asymptotic momentum of the electron with the molecular target in a state α. The (p,μ,α) indices in Equation (4) now label the symmetry and corresponding target state of the continuum wave function, and refer to the kernel of the integral operator $\hat{V}$, a sum of diagonal and nondiagonal terms that in principle fully describe the electron–molecule interaction during the collision. The choice of a single state α obtains the exact-static-exchange representation of the electron–molecule interaction for the molecular ground-state geometry $\mathbf{R}$ and is subsequently modeled by introducing the further assumption of having only a local electron–molecule interaction. Hence, one can simplify the form of the coupled equations

$$\left[\frac{d^2}{dr^2} - \frac{l_i(l_i+1)}{r^2} + k^2\right] f_i^{p\mu}(r|\mathbf{R}) = \sum_j V_{ij}^{p\mu}(r|\mathbf{R}) f_j^{p\mu}(r|\mathbf{R}), \quad (4)$$

where the indices i or j represent the angular channel (l, h), and the potential coupling elements are given by

$$V_{ij}^{p\mu}(r|\mathbf{R}) = \left\langle X_i^{p\mu}(\hat{\mathbf{r}})|V(\mathbf{r}|\mathbf{R})|X_j^{p\mu}(\hat{\mathbf{r}})\right\rangle = \int d\hat{\mathbf{r}} X_i^{p\mu}(\hat{\mathbf{r}}) V(\mathbf{r}|\mathbf{R}) X_j^{p\mu}(\hat{\mathbf{r}}). \quad (5)$$

The exchange contributions to the operator of Equation (5) are modeled with an energy-dependent local potential, the Hara free-electron gas exchange (Hara 1967), as discussed many times before (Telega & Gianturco 2005, 2006). As in several of our previous studies (Telega & Gianturco 2005, 2006), we further include the dynamical short-range correlation through the addition of a local energy-independent potential which is obtained by defining an average dynamical correlation energy of a single electron within the formalism of the Kohn and Sham variational scheme. The functional derivative of such a quantity with respect to the self-consistent field (SCF) approach N-electron density of the molecular target provides a density functional description of the required short-range correlation term that is an analytic function of the target electron density. The latter contribution is then connected with the long-range dipole polarizability term providing the additional polarization potential contribution, as given in detail by Lucchese & Gianturco (1996). The above modeling of the full interaction for an impinging electron on a many-electron molecular target has been used by us many times before, usually finding rather good agreement with the available experimental data (Lucchese & Gianturco 1996; Telega & Gianturco 2005, 2006; Carelli et al. 2008).

2.2. The Adiabatic Potential Model

Our main purpose in this paper is to investigate first the mechanism for the low-energy one-electron attachments to the o-C_6H_4 and possibly gain a deeper understanding of their qualitative features by an analysis of the spatial properties of the excess electron wave functions associated with the temporary anionic states. To do that, a model that is simple enough to be computationally attractive but, at the same time, includes sufficient details of the full scattering problem, is required: we want in fact to reproduce all the essential features of the physics involved within a limited computational effort. Thus, we look at the low-energy resonances using a purely local model potential that we have called the static model-exchange correlation (SMEC) potential, $V_{\rm SMEC}$ (Lucchese & Gianturco 1996). We start by noting that the standard, symmetry-adapted angular momentum eigenstates, $X_{lh}^{p\mu}$, do not actually form the most compact angular set for the electron–molecule scattering problem: an alternative basis expansion is provided, in fact, by the angular eigenfunctions obtained by diagonalizing the angular Hamiltonian at each radius r. These distance-dependent angular eigenstates are referred to as the adiabatic angular functions $Z_k^{p\mu}(\theta, \phi, r)$ which, at each radial value, are linear combinations of the symmetry-adapted "asymptotic" harmonics discussed before,

$$Z_k^{p\mu}(\theta, \phi, r) = \sum_{lh} X_{lh}^{p\mu}(\theta, \phi) C_{lh,k}(r), \tag{6}$$

where the expansion coefficients are solutions of the matrix eigenvalue equation

$$\sum_{lh} V_{l'h',lh}(r) C_{lh,k}(r) = C_{l'h',k}(r) V_k^A(r). \tag{7}$$

The eigenstates $V_k^A(r)$ now form an adiabatic radial potential for each index k over the selected range of the electron–molecule distances. The spatial extent of the resonant wave function can be determined from the well and angular momentum barrier of such adiabatic potential terms while the physical mechanism for the resonance is that of a trapped electron tunneling through the potential barrier. In order to also simplify the non-adiabatic coupling terms between adiabatic curves, we actually employ a piecewise diabatic (PD) representation of the potential by means of which the radial coordinate is divided into a number of regions so that the ith sector is defined as $r_{i-1} < r < r_i$, with $r_0 = 0$. In each radial region, we then average the coupling potential $V_{l'h',lh}(r)$ over r and the resulting averaged potential is diagonalized as in Equation (7) to yield a set of angular functions $Z_{k,i}^{p\mu}(\theta, \phi)$. Finally, in the ith radial region the scattering potential is transformed into the new representation in which it is nearly diagonal. The resulting equations are solved using the full scattering potential in each region with the further approximation of ignoring the off-diagonal couplings in that region; moreover, to solve the radial equations using the PD approach requires matching of both the radial functions and their derivatives at the boundary between each radial ith region. The transformation of the radial functions from one region to the next is given by the transformation matrix $U_{k,k'}^{(i+1\leftarrow i)}$ defined by

$$U_{k,k'}^{(i+1\leftarrow i)} = \sum_{lh} C_{lh,k}^{(i+1)} C_{lh,k'}^{(i)}. \tag{8}$$

When the size of the angular momentum eigenfunction basis used is larger than the size of the diabatic angular basis set, the transformation matrix $U_{k,k'}$ is not in general unitary. We accomplish the unitarization of $U_{k,k'}^{(i+1\leftarrow i)}$ using simple Graham–Schmidt orthonormalization on the columns of $U_{k,k'}^{(i+1\leftarrow i)}$.

3. RESULTS AND DISCUSSION

3.1. Numerical Details

Equilibrium structure, geometry optimizations, and the potential energy of the neutral species involved in this study, as well as the starting molecular orbitals (MOs) used for the present scattering calculations, have been performed at the HF/aug-cc-pVTZ level using the Gaussian suite of programs (Frisch et al. 2004). These ab initio calculations yielded for the title system a total SCF energy of −229.467905 hartrees. The molecular structure obtained with the above Gaussian basis-set shows good agreement with the earlier more accurate ab initio calculations (Groner & Kukolich 2006); see Figure 2 for their values. Using the above basis set, the calculated wave function for the neutral target yields a permanent dipole moment of 1.77 D, in good agreement with the theoretical value of 1.68 D (Kraka & Cremer 1993). According to the molecular symmetry point group to which the ortho-benzyne belongs at its equilibrium geometry, reported by Figure 2, the elastic cross sections and poles of the S-matrix for the scattering process,

$$\text{o-}C_6H_4(^1\Sigma) + e^- \rightarrow (\text{o-}C_6H_4^-)^*(^2A),$$

have been computed within the four IRs of the C_{2v} group using our scattering program (Lucchese et al. 1999): these calculations have been initially performed by us at the equilibrium geometry.

For the S-matrix calculations, we expanded the wave function up to a maximum angular momentum value of $L_{\rm Max} = 40$; the corresponding partial wave expansion for the scattering potential was thus carried out up to $l_{\rm MAX} = 80$; moreover, a maximum of 25 partial waves ($L_{{\rm Max}A} = 25$) was used by us for the corresponding scattering electron expansion within the PD potential approach. We note that to increase either values of the maximum angular momentum ($L_{\rm Max}$ and $L_{{\rm Max}A}$,

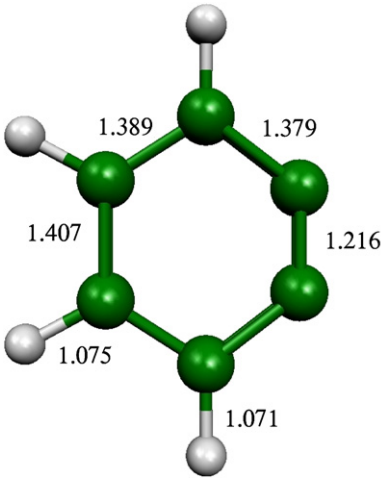

Figure 2. Computed geometry and bond values (in Å) for the title molecule. See the text for further details.

(A color version of this figure is available in the online journal.)

respectively, up to 60 and 30) had no significant effect on the final results. The size of the physical box that contains the diabatized partial terms, as described in the previous section, was 50 Å, then the overall radial and angular grids (r, θ, ϕ) included $1760 \times 80 \times 80$ points. The model correlation–polarization potential V_{cp} is the one described in our earlier work (Lucchese & Gianturco 1996; Telega & Gianturco 2005, 2006; Carelli et al. 2008); it was used in the present calculations with the total asymptotic polarizability value of 64.98 a_0^3 by us calculated. We shall describe below in greater detail how this term was included in our calculations.

3.2. The Integral Cross Sections

This section reports on our computed elastic (rotationally summed) integral cross sections for the equilibrium geometry of the title system. The actual energy behavior of the dominant symmetry components which make up the total electron scattering elastic cross sections is depicted in the energy range of interest within the three panels of Figure 3.

We report there the partial elastic cross sections for the a_2 (top panel), b_1 (middle panel), and b_2 (bottom panel) contributions; no maxima in the integral cross sections are found in the totally symmetric (a_1) component, the latter not being shown here. We are initially interested in revealing the possible existence of low-energy shape resonances in the o-C_6H_4 ($^1\Sigma$), features which are qualitatively due to short-range effects leading to dynamical trapping of the impinging electron. However, the ortho-benzyne molecule, due to its triple bond, has a large permanent electric dipole moment as well as a large spherical polarizability having their origin in the large number of π electrons in the aromatic pseudo-hexagonal ring. Thus, we cannot in principle discard the long-range polarizability contributions on the resonance parameters, and in the present case we indeed expect they shall play an important role in the scattering process.

Our long-range polarization potential contribution to the V_{cp} potential is obtained by using a potential form that asymptotically agrees with the value given by the static polarizability α of the molecule under investigation. This can be done either by assuming a single polarization center or by partitioning the static polarizability α on different centers where the individual atomic polarizabilities are subjected to the constraint that the total molecular polarizability is reproduced in the long-range region.

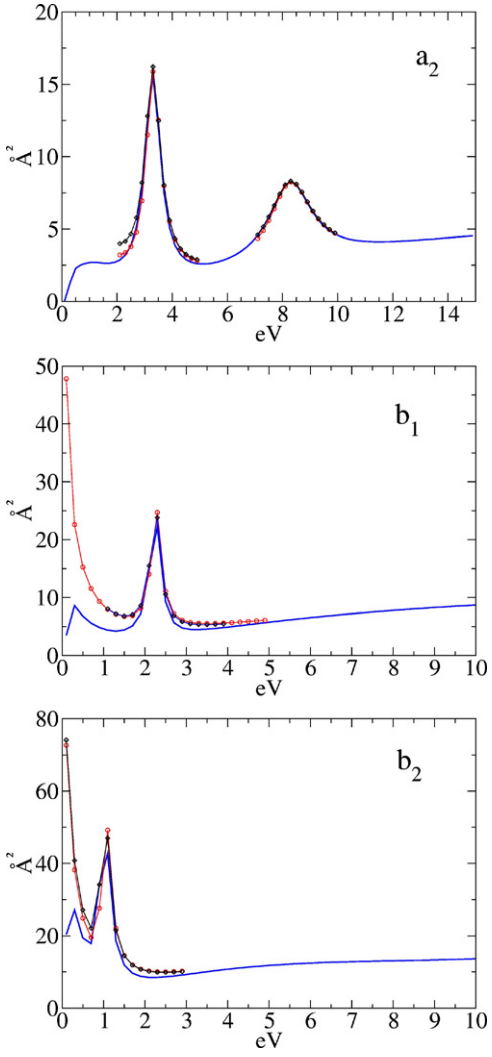

Figure 3. Computed elastic integral cross sections of the three molecular symmetry contributions. For the definition of the various curves shown, see the main text.

(A color version of this figure is available in the online journal.)

We have actually performed both such calculations including the long-range part of the electron–molecule interaction for all the elastic partial cross sections in the three contributing symmetries and also increasing the physical box up to 50 Å. The corresponding results are reported in Figure 2: the continuous lines represent the elastic partial integral cross sections computed without using the o-C_6H_4 ($^1\Sigma$) polarizability and at the same time referring to a physical box with a radius of 15 Å, while the circles and the diamonds refer respectively to a calculation which is now including either the spherical or the multicenter polarizability (the latter weighed and scaled by the Mulliken charges on each atomic center) as well as considering the larger physical box of 50 Å. We can immediately recognize that both the a_2 maxima and the higher energy maxima of b_1 and b_2 contributions appear at the energy values for which we also found the maxima without the dipole-induced polarization corrections. The situation is instead different for each of the very low energy features visible in the partial cross sections of b_1 and b_2 symmetries: when the polarizability is introduced in the calculation, they both disappear below threshold thus suggesting that they are actually artifacts created by the limited

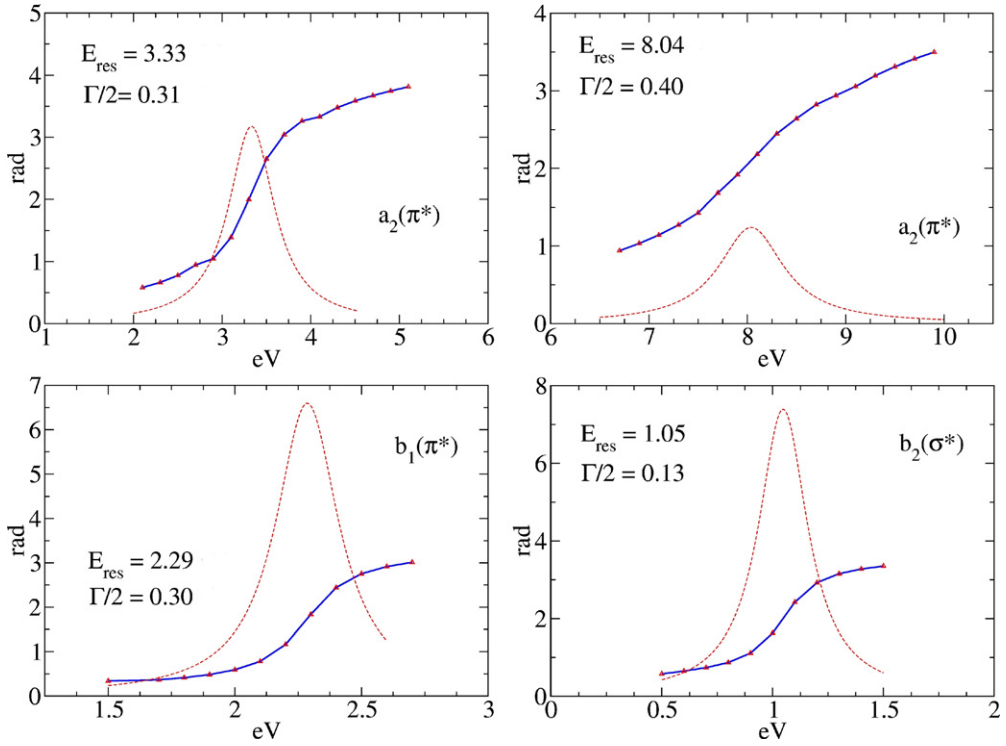

Figure 4. Computed eigenphase sums within each of the scattering contributions for the three symmetries discussed in the main text. All values are in eV.
(A color version of this figure is available in the online journal.)

size box employed initially. All further calculations were therefore done employing the larger integration "box" mentioned before (50 Å).

3.3. The σ^* and the π^* Resonances

We discuss below our results of the computed resonance parameters, i.e., the eigenphase sums and the diabatic potential curves, reported respectively in Figures 4 and 5. We are in fact interested in characterizing the metastable anions obtained from resonant trapping of the impinging low-energy electron because of their possible role as reaction intermediates in the circumstellar environment.

In Figure 4, we show the behavior of the eigenphase sums together with their first derivatives for each symmetry in which we find a maximum in the corresponding partial cross section. The four eigenphase sums were each fitted to a Breit–Wigner formula, using the familiar functional form (Taylor 1972)

$$\delta(E) = a + b(E - E_{\rm res}) + c(E - E_{\rm res})^2 + \arctan\left[\frac{\Gamma}{2(E - E_{\rm res})}\right] \quad (9)$$

in order to extract the pure resonant component from the background and to obtain the resonance width from the Lorentzian fit of the corresponding delay matrix. It is clearly seen that the four isolated resonant contributions in the three different symmetries, a_2, b_1, and b_2, show a sharp π jump when the collision energy of the charged projectile crosses the value for which each of the corresponding cross sections show a maximum, as discussed before: these findings confirm that the four maxima in the elastic partial cross sections correspond to pure shape resonances. The energy dependence of the lower components for each resonance is shown in the four panels of Figure 5, where angular momenta are reported up to $l = 3$ (b_1 and b_2 contributions) as well up to $l = 4$ (for the two a_2 resonances). We find it important to point out that the diabatic potential curves of the b_1 and b_2 symmetries are such that the corresponding impinging electron energies are in both cases degenerate with the minimum value needed to overcome their barriers; this particular feature is of importance in controlling the width of a resonance. The two resonances of the a_2 symmetry, as clearly shown in the two upper panels of Figure 5, are instead due to the tunneling across a barrier generated by the $l = 3$ (f wave) and $l = 4$ (g wave) angular momenta, features that therefore explain their being located at higher energies.

By examining the contour plots of the resonant wave functions of the three IRs in which we find shape resonances (which we do not report here for the sake of brevity), we have discovered that three of the four resonances have π^* nature (respectively, the two of the a_2 symmetry and the one of the b_1 symmetry), while the remaining b_2 resonance has σ^* nature.

The $b_2(\sigma^*)$ is now explicitly shown in Figure 6 and compared there with the nearest virtual MO obtained from the HF calculations on the target molecule. It shows that the distribution of electronic charge associated with the impinging electron is displaced asymmetrically, mainly on the carbon atoms of the triple bond where a nodal plane clearly exists perpendicular to that bond: this strongly suggests its antibonding behavior across this CC bond. Thus, according to these findings, the $b_2(\sigma^*)$ resonance at the equilibrium geometry could be reasonably considered a good candidate for adding antibonding behavior to the triple bond in the (N+1) electron system and therefore for being responsible for a possible ring-breaking process guided by the non-adiabatic coupling between this σ^* resonant electron and the nuclear dynamics which would then chiefly involve the triple bond. The following section shall further elaborate on this point.

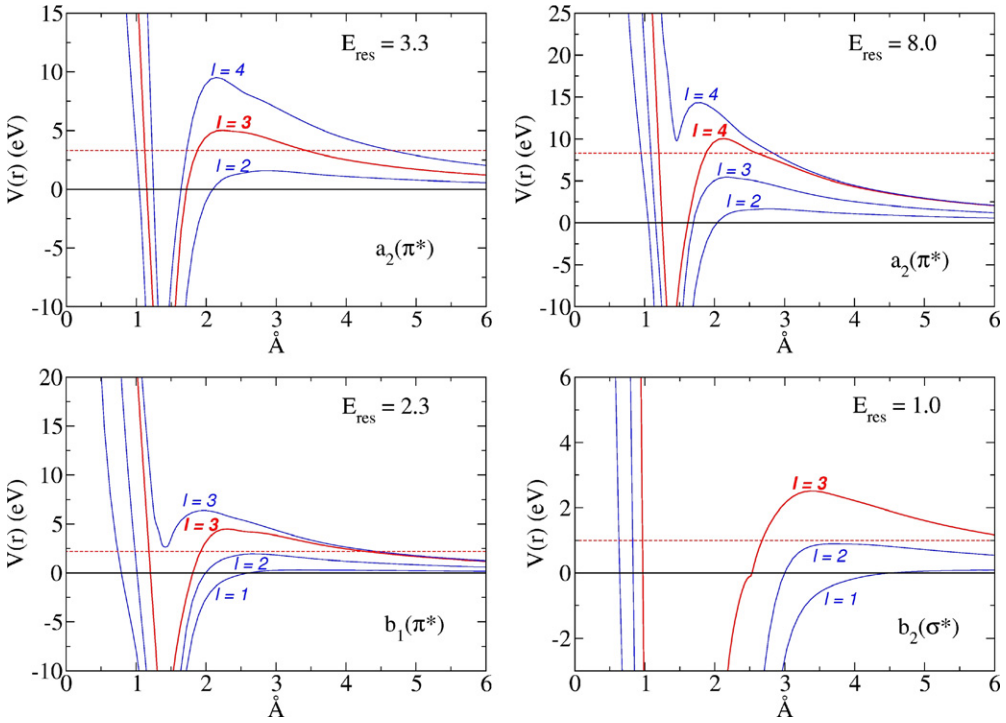

Figure 5. Computed diabatic potential energy curves employed for the calculation of each partial elastic integral cross section. See the main text for details. All energies are in eV.

(A color version of this figure is available in the online journal.)

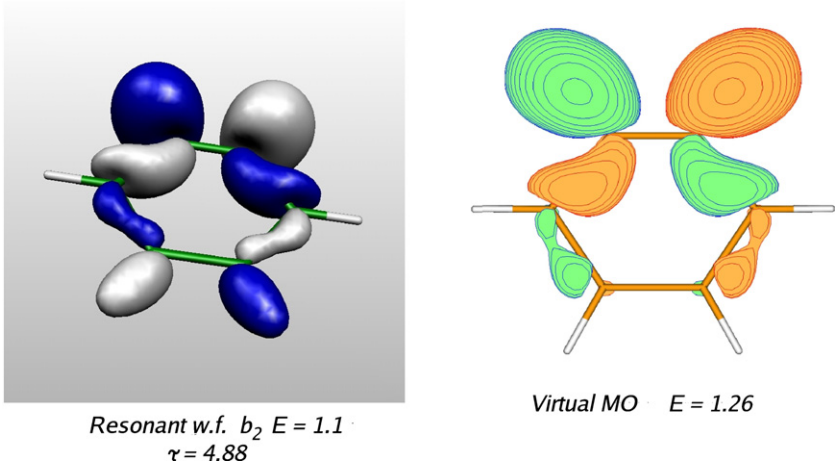

Figure 6. Left-hand panel: shape of the real part of the scattering wave function (w.f.) for the σ^* resonance computed using the PD model interaction. Right-hand panel: HF/aug-cc-pVTZ computed virtual MO of the ground electronic state of the o-C_6H_4 molecule for the b_2 symmetry where the σ^* resonance is located. All energy values in eV. The lifetime τ in units of 10^{-15} s.

(A color version of this figure is available in the online journal.)

3.4. o-C_6H_4 Versus C_6H_6: A Comparison Between Their Equilibrium Metastable Anions

From a structural point of view, one of the main differences between benzene and ortho-benzyne, both considered in their equilibrium geometries, lies in the lack for the latter of a vicinal couple of hydrogen atoms to which corresponds the presence of the triple bond. The ensuing appearance of a large permanent electric dipole moment (1.68 D) in the ortho-benzyne, in spite of the o-C_6H_4 and C_6H_6 having aromatic rings, turns out to be responsible, at least qualitatively, for many of the differences that we shall find below between the behavior of the resonant states of these molecules.

Let us briefly summarize the properties of the two systems.

1. The benzene molecule in its equilibrium geometry belongs to the D_{6h} symmetry group, while the ortho-benzyne belongs to the C_{2v}group.
2. Benzene is characterized by resonances in seven distinct IRs which correspond to symmetries for which there are no occupied MOs (a_{2g}, b_{2g}, and e_{2u}) as well as to symmetries where occupied MOs of the target ground electronic state exist (a_{1g}, e_{2g}, b_{1u}, and e_{1u}; Gianturco & Lucchese 1998).
3. According to the diabatic potential curves and to the eigenphase sums behavior as functions of the impinging electron energy, the first group of computed resonances

Table 1
Correlation Table $C_{2v} \leftarrow D_{6h}$ Between the Symmetry Groups Associated with Benzene D_{6h} and Benzyne C_{2v}

D_{6h}	C_{2v}
A_{1g}	A_1
A_{2g}	A_2
B_{1g}	B_1
B_{2g}	B_2
E_{1g}	$B_1 + B_2$
E_{2g}	$A_1 + A_2$
A_{1u}	A_2
A_{2u}	A_1
B_{1u}	B_2
B_{2u}	B_1
E_{1u}	$B_2 + B_1$
E_{2u}	$A_2 + A_1$

Table 2
Computed Resonances for the o-C_6H_4 Target

IR	E_{res}(eV)	Γ(eV)	$l_{dominant}$
b_2	1.05	0.27	2/3
b_1	2.29	0.61	2/3
a_2	3.33	0.63	3
a_2	8.04	0.81	4

Note. See the text for further details.

(Gianturco & Lucchese 1998) can be viewed as actual metastable negative ions of C_6H_6.

4. For the resonances which belong to an IR that also contains occupied MOs (with the exception of a_{1g} contribution), the corresponding diabatic potential curves indeed exhibit their lowest angular components with an l value greater than zero and located at rather low energy, thus having a barrier too low to support a shape resonance. In fact, each of their cross sections also shows one low-energy structure which could be qualitatively related to the top of the centrifugal barriers for the lowest contributing angular momenta (Gianturco & Lucchese 1998).

In order to make a more efficient comparison between the benzene and the ortho-benzyne resonances, we can use the correlation table $C_{2v} \leftarrow D_{6h}$ shown in Table 1. A first important difference between these molecules can be found in the fact that no resonance features appear in the totally symmetric contribution (a_1) for the ortho-benzyne, while for benzene two one-electron resonances both with symmetry a_{1g} (for which also bound MOs exist) can be identified.

Each of the partial cross sections in the b_1 and b_2 symmetries for o-C_6H_4 shows, as discussed before, that high-energy maxima do not undergo variation of their energy location once polarization effects are included. Moreover, their eigenphase sums as energy functions show a sharp π jump, thus indicating the dynamical trapping of the incident electron due to a non-adiabatic coupling between the $l = 2$ and $l = 3$ angular momentum contributions (see Table 2).

Through the above correlation table it is also possible to connect each of the four ortho-benzyne resonant states in Table 2 with those found for the C_6H_6 molecule (reported in Table 3). In general, however, with the exception of the a_2 (o-C_6H_4; $E_{res} = 8.0$ eV) $\rightarrow$ a_{2g} (C_6H_6; $E_{res} = 21$ eV) connection, which is geometrically rather simple to do, the remaining three metastable states for the ortho-benzyne molecule do not appear

Table 3
Computed Resonance Parameters for the Benzene Molecule as Reported in Gianturco & Lucchese (1998)

IR	E_{res}(eV)	Γ(eV)	$l_{dominant}$
e_{2u}	4.66	1.50	3
b_{2g}	9.02	2.26	4
e_{1u}	12.25	4.75	5
a_{1g}	12.32	6.78	4
e_{2g}	15.46	7.04	4
b_{1u}	16.52	12.81	5
a_{2g}	21.49	4.82	6
e_{1u}	21.96	14.63	5
b_{1u}	24.48	5.31	5
a_{1g}	25.73	10.09	6

to be comparable with any of those found for the benzene molecule in the calculations of Gianturco & Lucchese (1998). In other words, the removal of a vicinal couple of hydrogen atoms from the aromatic ring and the consequent presence of the large permanent electric dipole moment due to the triple bond make the resonant metastable states for the ortho-benzyne very distinctive, and it is then difficult to compare them with those found for the benzene, as they are in general different not only in the geometrical shape of the real parts of the resonant wave functions but are also associated with different dynamical mechanisms, as we shall further see below.

There are also additional differences that have to do with the global behavior of the metastable anions o-$C_6H_4^-$ and $C_6H_6^-$, both in their ground electronic states, as summarized in Tables 2 and 3. With the exception of the e_{2u} contribution, the benzene molecule exhibits resonances located at markedly higher energies than its ionization potential (9.24 eV; NIST 1993). Furthermore, the corresponding widths allow one to obtain for each benzene resonance a lifetime that is shorter than that associated with their nuclear vibration dynamics. The ortho-benzyne, on the other hand, appears to be somewhat more "reactive" in forming metastable anions: the ones calculated and discussed here correspond to energies that are well below its ionization potential (9.02 eV; Zhang & Chen 1992) and, as reported in the third Column of Table 3, the ortho-benzyne resonance widths are smaller, corresponding to greater lifetimes which then become comparable with the times for vibrational motions within the bound molecule.

On the basis of the above findings, we can therefore suggest that in the energy range of a few eV, which correspond to kinetic temperatures up to about 10,000 K for the circumstellar atmosphere of CRL 618 (Sanchez Contreras & Sahai 2002), the ortho-benzyne molecule could actually enter the complex chain of interstellar reactions by forming metastable anionic states more efficiently and less transiently than benzene.

4. CONCLUSIONS

The present study has been directed at the computational analysis of the possible role which could be played by the ortho-benzyne molecule as a reactive intermediate in proto-planetary atmospheres. In particular, we have studied the quantum dynamics of the scattering of low-energy (< 15 eV) electrons from gaseous o-C_6H_4 in order to verify its feasibility for forming long-lived negative ions as "doorway states" which can evolve through chemical reactions, leading to the formation of PAHs species.

The calculations have been carried out by treating the scattering events within a time-independent formulation of the problem, solving the ensuing multichannel equations within a SCE description of the scattering states and via a model, local potential for the interaction between the low-energy electrons and the benzyne molecules. The results indicate that the o-C_6H_4 indeed exhibits four fairly narrow resonances below 10 eV, three of which could be classified as π^* resonances while one of them is a low-energy σ^* resonance exhibiting antibonding character across the triple bond structure of the target molecule. Hence, we single out this resonance as the most likely dynamical mediator state which could conceivably lead to ring-opening processes. A comparison with similar scattering resonances which involve the benzene species (C_6H_6) indicates instead that the latter shows only fairly broad metastable states which start to appear above about 4.66 eV. Since the excess energy carried by the extra electron has to come from the environmental medium in the atmosphere, the attachment processes to benzene require much higher electron temperatures than those needed for the formation of metastable anions of benzyne. Furthermore, the latter temporary negative ions are seen to have longer lifetimes, thereby allowing more easily the dynamical coupling of the extra electron with the nuclear degrees of freedom which play a crucial role in the ensuing molecular breakup or ring-opening paths. It therefore follows that our present calculations support the picture of an intermediate anionic formation for benzyne that could rapidly decay by ring-opening reactions, a feature which therefore could prevent the actual detection of such anions by observational spectroscopy. Hence, we can say that the suggestion of a possible presence of o-C_6H_4 in proto-planetary atmospheres could in turn help in producing the negative, metastable species that would then be likely to contribute to the chain of reactions relevant for PAH formation. Such reactions would thus be more likely to be triggered by the latter molecule than by benzene itself, a feature that could then explain the observation of the latter neutral species (Cernicharo et al. 2001) with respect to the absence of the former one (Widicus Weaver et al. 2007).

One should keep in mind that the present calculations employ a realistic, but approximate, form of interaction and therefore possible experimental resonances would very likely be shifted in energy with respect to our estimates. On the other hand, our conclusions rest on having observed marked differences of behavior between the more stable resonant states of benzyne and those appearing at higher energy in benzene, a species considered to be the cornerstone step for the chain of reactions leading to PAH formation. Hence, the use in both cases of more realistic, improved model potentials would not modify our comparative conclusions.

In summary, we have shown that anionic formation for o-C_6H_4 is a very likely option in the circumstellar environment, a feature that would suggest its involvement with PAH reactions and formation in proto-planetary atmospheres. We intend to investigate further aspects of this problem with future work in our laboratory.

The financial support from the University of Rome Research Committee, Ministry of University National Research project PRIN 09, and the CASPUR Supercomputing Consortium is gratefully acknowledged.

REFERENCES

Agundez, M., et al. 2008, A&A, 478, 19
Altman, S. L., & Herzig, P. 1994, Point-group Theory Tables (Oxford: Oxford Univ. Press)
Carelli, F., Sebastianelli, F., Baccarelli, I., & Gianturco, F. A. 2008, Int. J. Mass Spectrom., 277, 155
Cernicharo, J., Heras, A. M., Tielens, A. G. G. M., Pardo, J. R., Herpin, F., Guelin, M., & Waters, L. B. F. M. 2001, ApJ, 546, L123
Cherchneff, I., Barker, J. R., & Tielens, A. G. G. M. 1992, ApJ, 401, 269
Frenklach, M., & Feigelson, E. 1989, ApJ, 341, 372
Frisch, M. J., et al. 2004, Gaussian 03 (Wallingford, CT: Gaussian Inc.), revision c.02
Gianturco, F. A., & Lucchese, R. R. 1998, J. Chem. Phys., 108, 6144
Groner, P., & Kukolich, S. G. 2006, J. Mol. Struct., 780, 178
Hara, S. 1967, J. Phys. Soc. Japan, 22, 710
Herbst, E. 1981, Nature, 289, 656
Kraka, E., & Cremer, D. 1993, Chem. Phys. Lett., 216, 333
Lucchese, R. R., & Gianturco, F. A. 1996, Int. Rev. Phys. Chem., 15, 429
Lucchese, R. R., Sanna, N., Natalense, A. P. P., & Gianturco, F. A. 1999, ePolyScat (version E2), http://www.chem.tamu.edu/rgroup/lucchese/ePolyScat.E2.manual/manual.html
McCarthy, M. C., Gottlieb, C. A., Gupta, H. C., & Thaddeus, P. 2006, ApJ, 652, L141
NIST. 1993, Computational Chemistry Comparison and Benchmark Database
Pardo, J. R., Cernicharo, J., & Goicoechea, J. R. 2007, ApJ, 661, 250
Sakai, N., Sakai, T., Osamura, Y., & Yamamoto, S. 2007, ApJ, 667, L65
Sanchez Contreras, C., & Sahai, R. 2002, ApJ, 578, 269
Sanchez Contreras, C., & Sahai, R. 2004, ApJ, 602, 960
Taylor, J. 1972, Scattering Theory. The Quantum Theory of Non-relativistic Collisions (New York: Wiley)
Telega, S., & Gianturco, F. A. 2005, Eur. Phys. J. D, 36, 271
Telega, S., & Gianturco, F. A. 2006, Eur. Phys. J. D, 38, 495
Tielens, A. G. G. M. (ed.) 2005, The Physics and Chemistry of the Interstellar Medium (Cambridge: Cambridge Univ. Press)
Widicus Weaver, S. L., Remijan, A. J., McMahon, R. J., & McCall, B. J. 2007, ApJ, 671, L153
Woods, P. M., Millar, T. J., Herbst, E., & Zijlstra, A. A. 2002, ApJ, 574, L167
Zhang, X., & Chen, P. 1992, J. Am. Chem. Soc., 114, 3147